Screen-printable microscale hybrid device based on MXene and layered double hydroxide electrodes for powering force sensors

Shuaikai Xu,[a] Yohan Dall'Agnese,[a] Guodong Wei,[a] Chao Zhang,[a] Yury Gogotsi[a,b]* and Wei Han[a,c]*

[a] *Key Laboratory of Physics and Technology for Advanced Batteries (Ministry of Education), Jilin University, Changchun, 130012, P. R. China*

[b] *Department of Materials Science and Engineering, and A. J. Drexel Nanomaterials Institute, Drexel University, Philadelphia, Pennsylvania 19104, USA*

[c] *International Center of Future Science, Jilin University, Changchun, 130012, P.R. China*

* Corresponding author.

E-mail addresses: gogotsi@drexel.edu, and whan@jlu.edu.cn

Abstract

Coplanar energy storage devices with interdigitated electrodes have attracted a significant amount of attention as micropower units for portable and flexible electronics, and self-powered systems. Herein, we propose a simple, cost-effective, and scalable two-step screen-printing process to fabricate flexible coplanar asymmetric microscale hybrid device (MHD) with a higher energy density compared to carbon-based microsupercapacitors. 2D titanium carbide MXene ($Ti_3C_2T_x$) with a large inlayer spacing is selected as negative electrode, and Co-Al layered double hydroxide (LDH) nanosheets are selected as positive electrode. The assembled coplanar, all-solid-state, asymmetric MHD possesses a higher energy density (8.84 μWh cm^{-2}) compared to the MXene-based, coplanar, symmetric microsupercapacitors (3.38 μWh cm^{-2}), and exhibit excellent flexibility and reliability, as well as cycling stability (92% retention of the initial capacitance after 10,000 cycles). Moreover, we integrate the coplanar asymmetric MHDs with the force sensing resistors as portable power source units to fabricate lightweight and inexpensive integrated force sensors, which can be used to detect applied pressure variation. The two-step screen-printing method can also be extended to other MXenes and various positive electrode materials for fabrication of coplanar asymmetric MHDs on flexible substrates. Therefore, we believe that the two-step screen-printing method opens up new avenues toward developing flexible coplanar asymmetric MHDs, thus promoting the application of MHDs based on MXenes for flexible integrated electronic devices.

Keywords: MXene; layered double hydroxide; screen-printing; microscale hybrid device; force sensor.

1. Introduction

With the rapid development of miniaturized portable, flexible, and stretchable electronic devices, especially integrated self-powered smart devices that can enable the "internet of things", micro-/nanoscale energy storage units have become increasingly important [1-3]. Tremendous efforts have been made to develop thin film microbatteries and microsupercapacitors [4-7]. However, when integrated with the functional sensing/detecting or other functional components as a power source, the energy storage units usually need charge or discharge at variable "non-constant" currents, depending on the response to the external force, temperature, illumination, etc. Compared to microbatteries, which suffer from low power density and short cyclic lifetime, a supercapacitor with high power density and long cyclic lifetime is a better choice for applications in integrated multifunctional systems. In this scenario, coplanar microsupercapacitors with predesigned electrode architecture can be integrated on the same substrate as other electronic components, such as sensors or rectifiers [8].

Conventional microfabrication techniques have been widely employed in fabricating electrical double layer type microsupercapacitors [7-13] using various carbonaceous materials (activated carbon [14], carbide derived carbon [15], onion-like carbon [16], and graphene [17]), which usually present low energy density due to the electrostatic ion adsorption mechanism. Furthermore, pseudocapacitive materials such as transition metal oxides [18], hydroxides [19], layered double hydroxides [20], and conducting polymers [12], in which charge storage is due to the fast near-surface redox reactions, were used in enhancing the energy density of on-chip electrochemical devices. However, pseudocapacitors usually suffer from short cyclic lifetime due to the poor nanostructure stability of the pseudocapacitive materials. Recently, MXenes, a new family of two-dimensional layered transition metal carbides or nitrides, have shown great promise as potential electrode materials for electrochemical energy storage devices [21-24]. Various ions can rapidly intercalate between MXene atomic layers (intercalation pseudocapacitance), resulting in high capacity, even at high discharge rates [25, 26]. $Ti_3C_2T_x$ is the most studied

member within the family of MXenes due to its great conductivity (up to 6500 S cm^{-1}), surface hydrophilicity, and excellent ion intercalation behavior [27]. Kurra et al. reported a direct laser machining process to fabricate MXene on-paper coplanar microsupercapacitors [10]. Peng et al. fabricated all-MXene ($Ti_3C_2T_x$) solid-state interdigital microsupercapacitors by employing a solution spray-coating method, followed by a photoresist-free direct laser cutting method [11]. Typical areal capacitance of 25 mF cm^{-2} for the MXene based microsupercapacitors is superior to the areal capacitance of various carbon-based microsupercapacitors reported in the literatures (0.1-10 mF cm^{-2}) [14-17]. However, the energy density of the MXene-based symmetric devices is restricted by the narrow working potential window, which also limits their practical applications when integrated with other functional electronic units. Energy density enhancement can also be achieved by fabricating asymmetric or hybrid devices, improving the working potential window, and incorporating a battery-like electrode material capable of storing large charge due to electron transfer within the anodic potential window complementing that of MXene [28-30]. Therefore, an optimized positive material with faradaic pseudocapacitance behavior is required to assemble an asymmetric hybrid device with MXene as negative electrode. In the last few decades, metallic layered double hydroxides (LDHs) with the general chemical formula $[M^{2+}_{1-x}M^{3+}_{x}(OH)_2]^{x+}[A^{n-}]_{x/n}\cdot mH_2O$, where M^{2+} and M^{3+} are divalent and trivalent metal cations and A^{n-} are the charge-balancing anions, have been proven to be a promising class of electrode materials for energy storage because of their relatively low cost and high redox activity [31, 32]. Co-Al LDH, among many LDHs, is a promising candidate for positive electrodes due to its high charge storage capacity. Gao et al. demonstrated that Co-Al LDH with high specific capacitance could be combined with graphene to assemble asymmetric supercapacitors [33]. However, the cycling stability of LDHs is usually poor because of the re-stacking of 2D nanosheets. Fabrication of LDHs with three-dimensional (3D) hierarchical structure may to impede the re-stacking of 2D nanosheets [34]. Moreover, the reported fabrication methods of asymmetric MHDs are usually costly and time consuming, therefore the development of a simple, scalable, and cost-effective

method is important. Typically, screen-printing method, being one of the most important and powerful industrial techniques is inexpensive, rapid, and facilitates mass production [35, 36]. Furthermore, screen printing allows for control over the deposition area and the ink can be printed on a wide variety of substrates, including paper, fabrics, and plastics.

Herein, we assembled coplanar asymmetric MHDs with $Ti_3C_2T_x$ and Co-Al-LDH electrodes by modified two-step screen-printing process. Clay-like $Ti_3C_2T_x$ with intercalated Li^+ ions as a result of LiF-HCl etching possesses high electrochemical performance due to larger interlayer spacing and was selected to serve as the negative electrode [27]. The Co-Al-LDH nanosheets with 3D hierarchical structure were synthesized by soft-template method and used as the positive electrode. $Ti_3C_2T_x$ and Co-Al-LDH nanosheets were screen-printed on paper and polyethylene terephthalate (PET) substrates to fabricate coplanar asymmetric MHDs with interdigitated electrode architecture. The areal capacitance reached ~40.0 mF cm^{-2} (at 0.75 mA cm^{-2}) and ~28.5 mF cm^{-2} (at 0.75 mA cm^{-2}) for the fabricated asymmetric MHDs in 6 M KOH and PVA-KOH gel electrolyte, respectively. The assembled flexible, all-solid-state asymmetric MHDs are found to have superior areal energy and power densities (the energy density of 8.84 μWh cm^{-2} at a power density of 0.23 mW cm^{-2}) compared to reported state-of-the art MXene-based MHDs. In addition, the coplanar asymmetric MHDs were integrated with the force sensing resistors as portable power source units to fabricate lightweight and inexpensive integrated force sensors, which were used to detect applied pressure variation. Notably, the two-step screen-printing method can also be extended to other MXenes and various positive electrode materials for fabrication of coplanar asymmetric MHDs, which promotes the development of MXene-based MHDs and their integration with other portable multifunctional electronic systems.

2. Experimental section

2.1. Synthesis of Co-Al-LDH nanosheets

In a typical procedure, 2.4 mmol $Co(NO_3)_2 \cdot 6H_2O$ and 0.8 mmol $Al(NO_3)_3 \cdot 9H_2O$ were dissolved in 80 mL mixed deionized water/butyl alcohol solvent (volume ratio =

1:1) and stirred for 30 minutes. Then, 0.384 g of urea and 15 mg of citric acid trisodium salt dehydrate were added and further stirred for another 30 min. Next, the mixtures were sealed in a 100-mL Teflon-lined steel autoclave and hydrothermally treated at 120 ˚C for 12 h. After being cooled to room temperature, the samples were filtered and washed with deionized water and ethanol several times and then freeze-dried for 24 h to obtain Co-Al-LDH with 3D hierarchical structure built of thin LDH nanosheets.

2.2. Synthesis of $Ti_3C_2T_x$

Commercially available TiH_2, Al, and TiC powders were used without any further purification to synthesize the MAX phase layered ternary carbide, Ti_3AlC_2. TiH_2, Al, and TiC were mixed in 1: 1.2: 2 molar ratio, ball milled for 24 h followed by sintering in a tube oven at 1450 ˚C in a corundum crucible and kept at that temperature for 2 h in a flowing Ar atmosphere. The resulting loosely held compact powder was crushed and sieved through a 400 mesh to obtain Ti_3AlC_2 powder with particle size of < 38 μm. $Ti_3C_2T_x$ was prepared by following the procedure reported elsewhere [27]. 3 g of LiF was added into 60 mL of 12 M HCl, and the solution was stirred for 10 min for homogeneous mixing. Then, 2 g of Ti_3AlC_2 MAX powder was immersed into the solution and kept at 40 °C for 45 h under constant stirring. The resulting suspension was washed several times with deionized water and centrifuged to separate the supernatant. The $Ti_3C_2T_x$ prepared by this method contained intercalated Li^+ ions and was referred to as $Ti_3C_2T_x$ in this study.

2.3. Screen-printing of MHDs

Commercially available A4 printing paper and polyethylene terephthalate (PET) film were used as flexible substrates to screen-print MHDs. An Au layer of ≈200 nm thickness was deposited on the substrates by magnetron sputtering and then carved to form predesigned current collector patterns with the help of direct laser machining. Homogenous active material inks were prepared by mixing the active material with acetylene black and polyvinylidene fluoride (PVDF) in N-methyl-2-pyrrolidone (NMP) solvent. Subsequently, a modified two-step screen-printing process was applied to fabricate asymmetric MHDs. During the printing of negative electrodes, the

screen was placed a few millimeters above the surface of the substrate. After loading the MXene ink on the screen, a rubber squeegee was swept across the surface of the screen, bringing the ink into close contact with the substrate. At the same time, the ink flowed from the screen to the surface of the substrate. The screen was then separated from the substrate, leaving behind ink that dried to yield an electrode with mass loading of ~1 mg cm^{-2}. The positive electrodes were then screen-printed by a similar procedure. Finally, flexible asymmetric MHDs with interdigitated electrode architecture were fabricated on PET and paper. For comparison, symmetric MXene-based microsupercapacitors were also prepared by one-step screen-printing process.

2.4. Preparation of gel electrolyte

The PVA-KOH gel electrolyte was prepared as follows: Approximately 3 g of PVA was weighed and transferred into 30 mL of deionized water. The mixture was heated at 90 ˚C with constant stirring until a transparent solution of PVA was obtained. The solution was then cooled to room temperature. Approximately, 3 g KOH was dissolved in 10 mL H_2O and was added to the PVA solution and stirred gently to obtain homogeneous PVA-KOH gel electrolyte.

2.5. Assembly of all-solid-state MHDs devices

PVA-KOH gel electrolyte was carefully drop casted onto the coplanar asymmetric MHDs, then the devices were slowly dried at room temperature to form solid films. Similarly, symmetric MXene-based microsupercapacitors were covered with PVA-KOH gel electrolyte.

2.6. Assembly of the integrated force sensor

The force sensor (FSR 400 short tail model, Interlink Electronics, Inc.) was connected in series with the coplanar asymmetric MHD using conductive silver paint to fabricate the integrated force sensor. The force sensor is a polymer thick film device which exhibits a decrease in resistance with an increase in the force applied to its surface.

2.7. Material characterization

The $Ti_3C_2T_x$ powders and Co-AL-LDHs nanosheets were characterized using a

powder X-ray diffractometer (XRD, Bruker, D8 ADVANCE) with Cu Kα radiation (λ = 0.15406 nm). The morphology of the materials was characterized using a MEGALLAN 400 scanning electron microscope (SEM) and a transmission electron microscope (TEM) (JEOL JEM-2100, Japan), with an accelerating voltage of 200 kV. The TEM samples were prepared by placing several drops of the sample dispersion in alcohol onto a copper grid and air drying. X-ray photoelectron spectroscopy (XPS) was used to characterize the synthesized Co-Al-LDHs. The atomic composition of Co-Al-LDHs nanosheets was analyzed using energy dispersive spectroscopy (EDS).

2.8. Electrochemical measurement

The electrochemical tests (cyclic voltammetry (CV), galvanostatic charge-discharge (GCD), electrochemical impedance spectroscopy (EIS)) were carried out at room temperature using an electrochemical working station (IVIUMSTAT A11719). Cyclic performance measurements were carried out using a battery test system (LAND CT2001A model, Wuhan Jinnuo Electronics. Ltd., China). The EIS was measured in the frequency range from 100 kHz to 10 mHz at open circuit potential by applying a small sinusoidal potential of 10 mV signal. For three-electrode measurement, $Ti_3C_2T_x$ and Co-Al-LDHs were employed as working electrode, platinum foil as the counter electrodes, and saturated calomel electrode (SCE) as reference electrodes. The working electrodes were prepared as follows: The active materials were mixed with acetylene black and PVDF in a weight ratio of 8:1:1 in NMP solvent to form homogenous slurry. Then the slurry was pressed on Ni foam with mass loading of $\approx$2 mg cm^{-2} and dried at 60 ˚C under vacuum. The electrochemical performance of the assembled MHDs was investigated in two-electrode configuration. The fabricated MHDs were connected to copper tape using silver paste. The fabricated asymmetric MHDs devices were tested in 6 M KOH and PVA-KOH gel electrolyte, and the symmetric MXene-based microsupercapacitors devices were tested with PVA-KOH gel electrolyte. The calculation methods for areal capacitance, energy density, and power can be found in supporting information. The current signal of the integrated force sensor was measured using CHI760E electrochemical workstation, where the amperometric *i-t* curve technique was selected.

Four weights (20 g, 50 g, 100 g and 200 g) were used to apply different forces (0.2 N, 0.5 N, 1 N and 2 N) to the surface of the force sensor. The heart rate was measured by touching the surface of the force sensor, which could detect the weak pulsation of blood in a finger.

3. Results and discussion

The process for the fabrication of the coplanar MHDs are shown in Fig. 1. An Au layer of ≈200 nm thickness was deposited on the flexible substrates by magnetron sputtering and then carved to form predesigned patterns with the help of direct laser machining, which was employed as current collector (Fig. 1a, 1d). To fabricate asymmetric MHDs, positive electrode (Co-Al-LDH nanosheets) was first screen-printed on the substrates (Fig. 1b). After air drying, the negative electrode (MXene) was screen-printed to form a coplanar asymmetric MHD with predesigned electrode architecture (Fig.1c). Similarly, symmetric MXene-based microsupercapacitors were also fabricated by one-step screen-printing process (Fig. 1e). In this work, the MHDs with interdigitated electrode architecture were produced and electrochemically characterized. The schematic diagram of the employed screen-printing plates is shown in Fig. S1. Fig. S2a shows that the width of a finger electrode is around 1 mm (spacing between the fingers is also 1 mm). A low-magnification SEM image presented in Fig. S2b shows that the electrode material (MXene with mass loading of ≈1 mg cm^{-2} in this case) effectively adheres to the surface of paper due to intrinsically rough and porous morphology of the latter. As shown in Fig. 1f, MHDs on both paper and PET substrates, possess good flexibility. Compared to the conventional microfabrication techniques [7, 8, 13, 17, 37], the modified two-step screen-printing method is simple, cost-effective, and scalable. Furthermore, screen-printing allows for good control over the deposition area, and the ink can be printed on a wide variety of substrates, including paper, fabrics, and plastics.

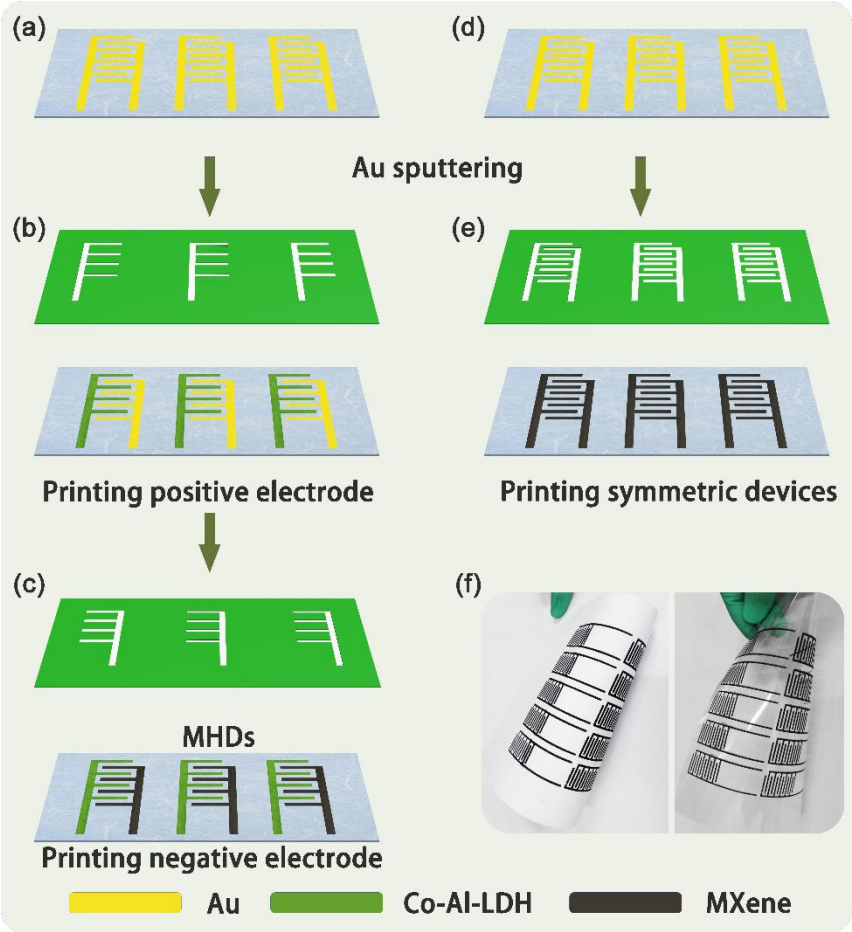

Fig. 1. Schematic illustration of the screen-printing process of the flexible MHDs on flexible substrate (PET and commercial printing paper). (a, d) Sputtering gold with predesigned pattern on the substrate. (b, c) Fabrication of asymmetric MHDs by modified two-step screen-printing process. (e) Screen-printed symmetric microsupercapacitors based on MXene. (f) Digital photographs of the fabricated coplanar MHDs on commercial printing paper (left) and PET (right).

LiF dissolved in HCl was used as etching solution to synthesize $Ti_3C_2T_x$. During the etching of Al layers, the Li^+ ions from LiF intercalate between oxygen-containing functional groups (-O, -OH and -F) of terminated MXene layers, resulting in tightly stacked flakes (Fig. S3b) with clay-like rheological behavior [27, 38]. Fig. 2a shows the schematic of the $Ti_3C_2T_x$ structure. The XRD patterns of Ti_3AlC_2 and $Ti_3C_2T_x$ are presented in Fig. 2b. It can be observed that after etching of Al layers using LiF/HCl, the most intense peak at $2\theta = 39.3^\circ$ disappears, indicating that Al layers were completely etched away. In addition, the (0002) peaks for $Ti_3C_2T_x$ became broadened

and shifted to the lower angle as compared to that of Ti_3AlC_2 MAX phase, which is attributed to the loss of correlation between the layers and increases in c-lattice parameter due to the intercalation of Li^+ ions and water molecules [27]. The large d-spacing can promote the intercalation and transport of electrolyte ions. Furthermore, from the TEM image (Fig. 2c) it can be observed that the $Ti_3C_2T_x$ nanosheets are flat and unbroken. The selected area electron diffraction (SAED, inset in Fig. 2c) exhibits a typical six-fold symmetric diffraction pattern, indicating the high crystallinity of $Ti_3C_2T_x$. Co-Al-LDH with 3D hierarchical structure were synthesized by soft-templating method and used as positive electrode for fabricating MHDs. The SEM image in Fig. S4a presented the 3D hierarchical structure built of thin LDH nanosheets. This morphology was further confirmed by TEM (Fig. 2f). The selected area electron diffraction (SAED, inset in Fig. 2f) indicates the high crystallinity of Co-Al-LDH. The schematic of the Co-Al-LDH structure is shown in Fig. 2d. When Co-Al-LDH is synthesized using mixed water/butyl alcohol solvent, the formation of a 3D structure built of thin LDH nanosheets can be explained as follows: during the reactions, the selective adsorption of butyl alcohol molecules on the (001) planes of Co-Al-LDH minimizes the surface energy to form and stabilize thin LDH nanosheets [39]. Furthermore, the interactions of butyl alcohol adsorbed on the surface of the LDH nanosheets can also promote the formation of 3D hierarchical structure by the self-assembly of thin LDH nanosheets, following co-precipitation, dissolution and recrystallization processes. The 3D hierarchical structure built up of LDH nanosheets could facilitate the diffusion of electrolyte into the electrodes and improve the electrochemically active area [34]. Co-Al-LDH was then combined with another 2D material capable of large energy storage (MXene) for fabricating MHDs with enhanced electrochemical performance. The XRD pattern was carried out to reveal the phase composition and crystallinity of the Co-Al-LDHs (Fig. 2e). From the diffraction peaks location, it can be confirmed that Co-Al-LDHs have a rhombohedral structure and evident crystallinity [31]. The stable atomically thin LDH nanosheets and their crystalline character will benefit the cyclic performance of Co-Al-LDHs electrodes. The EDS spectra and XPS spectra of Co-Al-LDH were recorded to

investigate the atomic composition and chemical states of elements, as described in Supporting Information (Fig. S4b, Fig. S5).

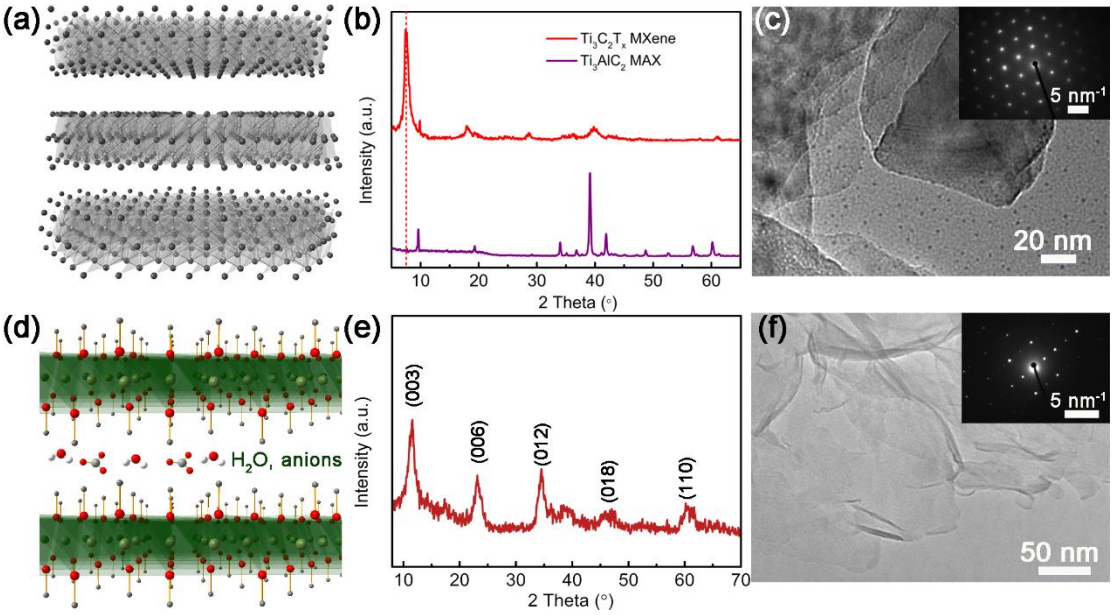

Fig. 2. (a) Schematic of the $Ti_3C_2T_x$ structure. (b) XRD patterns for clay-like $Ti_3C_2T_x$ in comparison to the bulk MAX phase, Ti_3AlC_2. (c) TEM image of $Ti_3C_2T_x$ nanosheets, the inset is the corresponding SAED pattern. (d) Schematic of the Co-Al-LDH structure. (e) XRD patterns for Co-Al-LDH. (f) TEM image of Co-Al-LDH nanosheets, the inset is the corresponding SAED pattern

When fabricating asymmetric MHDs, the mass loading of negative and positive electrodes should be balanced according to the charge balance between the two electrodes [40-42]. Therefore, the electrochemical performances of $Ti_3C_2T_x$ and Co-Al-LDH nanosheets were measured in three-electrode configuration prior to fabricating MHDs. As shown in Fig. 3a, the CV curves of $Ti_3C_2T_x$ at different scan rates present quasi-rectangular profiles, even at high scan rate of 100 mV s^{-1}. This is attributed to the intercalation of Li^+ and H_2O molecules between $Ti_3C_2T_x$ layers results in larger layer spacing, promoting the diffusion and intercalation of electrolyte ions. As shown in Fig. 3b, the GCD curves of $Ti_3C_2T_x$ are linear and symmetric with a small IR drop, indicating its typical capacitive behavior, which is in agreement with the results of CV curves. The specific capacitance of $Ti_3C_2T_x$ calculated from the galvanostatic discharge curves reached 52 F g^{-1} at current density of 1 A g^{-1} in 6 M KOH. To

further understand the ion-transport behavior and electrical resistance of $Ti_3C_2T_x$, EIS was carried out in 6 M KOH. It can be observed that the Nyquist plots (Fig. 3c) exhibit typical capacitive-type impedance in a quite wide frequency region, representing the highly reversible cations insertion into the electrodes.

As shown in Fig. 3d, the CV curves of Co-Al-LDHs at different scan rates show broad oxidation/reduction peaks, but the peak separation is moderate, indicating that Co-Al-LDHs possess redox behavior that is close to pseudocapacitive behavior. Furthermore, it can be observed that at both poles of the potential window, the polarity of responsive current can immediately change to the contrary, indicating that the diffusion limitations in the electrode are moderate. The GCD curves at different current densities (Fig. 3e) show symmetric triangle profile, further demonstrating the enhanced capacitive performance. At current density of 6 A g^{-1}, the gravimetric capacitance of Co-Al-LDHs electrode is 766 F g^{-1}, and even at 50 A g^{-1}, the value remains 701 F g^{-1} (91.5% of the initial value at 6 A g^{-1}). The Nyquist plots (Fig. 3f) showed linearity with high slope value in the low frequency region, indicating the typically capacitive-type impedance of Co-Al-LDHs. The small semi-circle in the high-frequency region (inset in Fig. 3f) indicates that the prepared Co-Al-LDHs electrodes exhibit a low charge transfer resistance, which is attributed to the 3D hierarchical structure built up of thin LDH nanosheets.

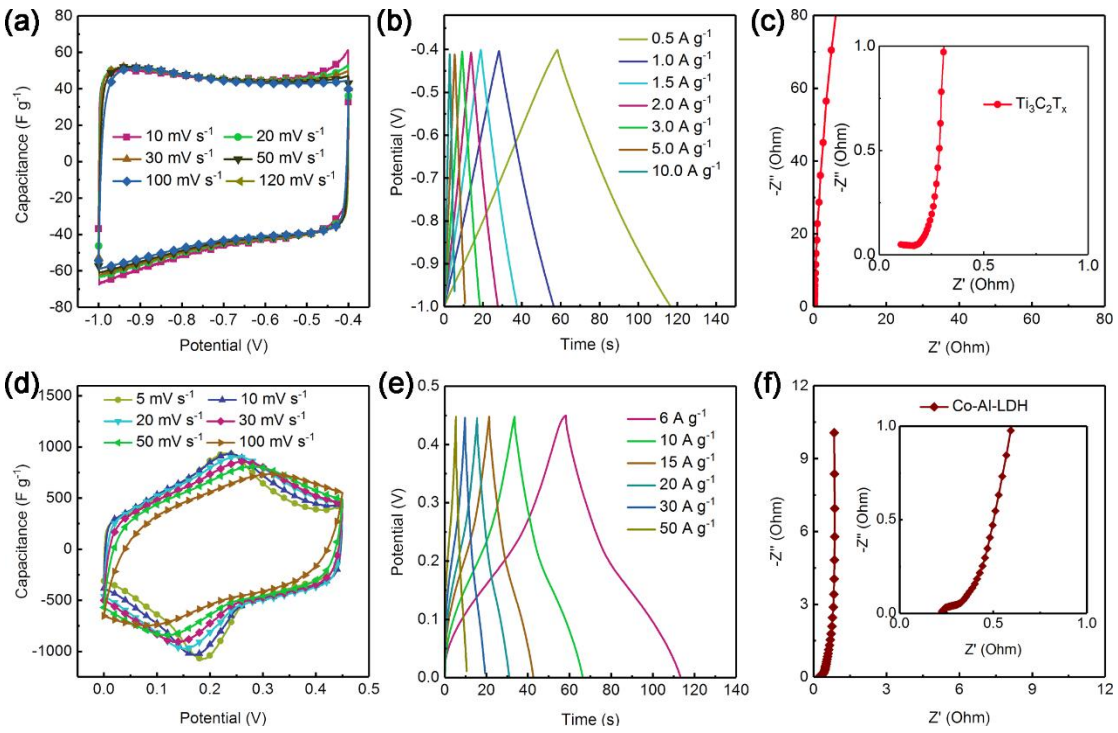

Fig. 3. Electrochemical performance of $Ti_3C_2T_x$ and Co-Al-LDH nanosheets in three-electrode configuration. (a, b) CVs at different scan rates and GCDs at different current densities for $Ti_3C_2T_x$ in 6 M KOH, respectively. (c) The EIS spectra of $Ti_3C_2T_x$ in 6 M KOH. (d, e) CVs at different scan rates and GCDs at different current densities for Co-Al-LDH in 6 M KOH, respectively. (f) The EIS spectra of Co-Al-LDH in 6 M KOH.

Asymmetric MHDs were fabricated by modified two-step screen-printing process and denoted as $Ti_3C_2T_x$//Co-Al-LDHs. The interdigitated electrodes of the MHDs result in efficient charge transfer and mass transfer between the electrodes: (1) the sputtered Au layer can serve as good current collector for the transport of electrons, (2) the ions in electrolyte can efficiently transport due to the interdigitated electrode architecture and short paths between the finger electrodes. From the CV curves (in 6 M KOH) of the asymmetric MHD operated in different voltage windows at a scan rate of 30 mV s^{-1} (Fig. 4a), it can be seen that the potential window of the asymmetric MHDs devices can be extended to 1.45 V without obvious oxygen evolution (no sudden rise in the current at higher potentials). Fig. 4b shows the CV curves of MHDs in 6 M KOH at different scan rates from 10 mV s^{-1} to 100 mV^{-1} between 0.4 and 1.45

V. The type of the electrochemical behavior of MHDs can be qualified as pseudocapacitive due to the fast quasi-rectangular response even at a high scan rate of 100 mV s^{-1}. The quasi-rectangular profiles of CVs indicated that the charges stored in the positive and negative electrodes were well balanced [43]. To further demonstrate that the two electrodes are balanced, the asymmetric MHD was tested in three electrode system, and the potentials of the positive and negative electrodes of the asymmetric MHD versus reference electrode were recorded. As shown in Fig. 4c and d, the potential-current curves of two electrodes of the asymmetric MHD all present quasi-rectangular profiles, proving that there is a great balance between positive and negative electrodes. In addition, the ranges of voltage variations of MXene and Co-Al-LDH were consistent with their potential windows used in the three-electrode system (results in Fig. 3), indicating that the asymmetric MHD can be stably charged-discharged between 0.4 V and 1.45 V. Furthermore, from the corresponding potentials for the positive and negative electrodes in Fig. 4e, it can be observed that the voltages of the asymmetric MHD were 0.4 and 1.45 V at end of discharge and charge, respectively, which is consistent with the result of the GCD curve of the asymmetric MHD (black curve in Fig. 4e). All the aforementioned results demonstrated that two electrodes of the asymmetric MHD were exactly balanced. The capacitive behavior of $Ti_3C_2T_x$//Co-Al-LDHs in 6 M KOH can be further confirmed from the quasi-linear profiles of the GCD curves shown in Fig. S6. From the galvanostatic discharge curves, the areal capacitance of the asymmetric MHD calculated, based on the total area of both electrodes, reached 40.0 mF cm^{-2} at a current density of 0.75 mA cm^{-2}. Even at a higher current density of 2.5 mA cm^{-2}, the areal capacitance still remained 31.2 mF cm^{-2}. To further develop the device fabrication, integration of series and parallel connections was investigated with the asymmetric MHDs. As shown in Fig. 4f, the series-connected devices gave lower areal capacitance values, but a higher voltage of 2.9 V. However, parallel configuration increased

the areal capacitance in the same voltage window, showing how in-series and parallel designs are beneficial for practical applications.

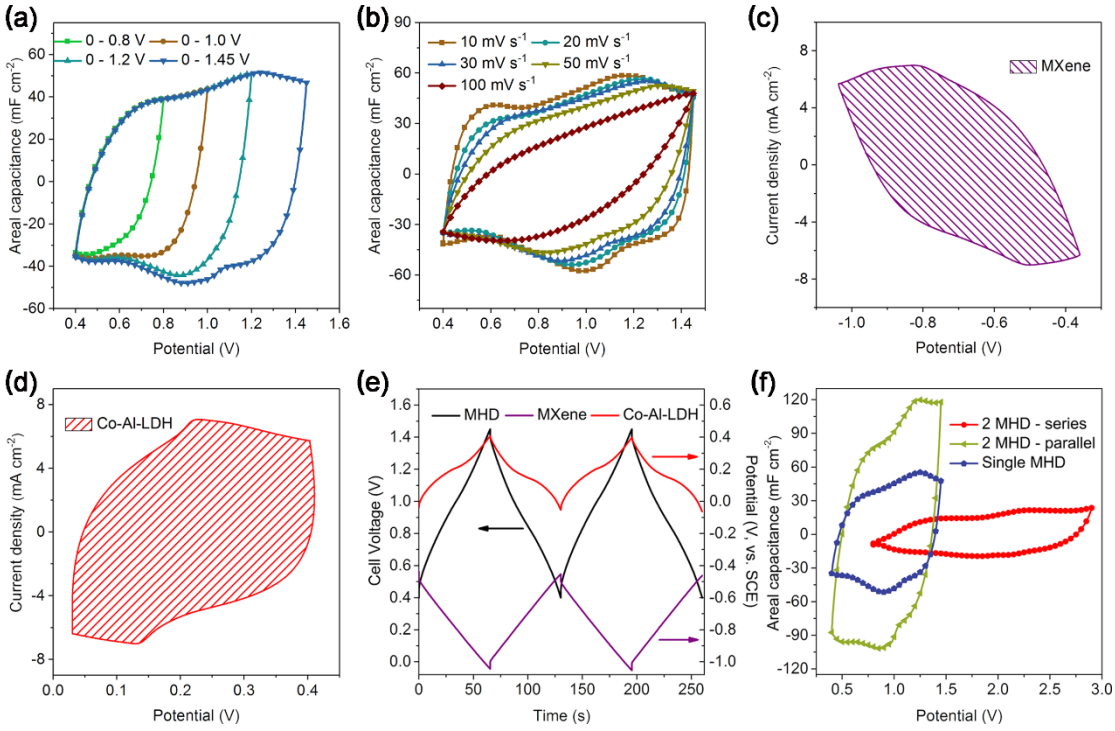

Fig. 4. (a) CV curves of the asymmetric MHDs in 6 M KOH electrolyte at different voltage windows at 30 mV s^{-1}. (b) CV curves of asymmetric MHDs at different scan rates in 6 M KOH. (c, d) The corresponding CV curves of negative ($Ti_3C_2T_x$) and positive (Co-Al-LDH) electrodes of an asymmetric MHD tested at 50 mV s^{-1}. (e) The GCD curves of an asymmetric MHD (left Y-axis) and corresponding potentials for the positive and negative electrodes (right Y-axis) at 1.25 mA cm^{-2}. (f) Comparison of CV curves (in 6 M KOH) for a single asymmetric MHD and two MHDs connected in series and parallel configurations at 30 mV s^{-1}.

With the aim of developing flexible and lightweight power source units for integrated portable electronics, all-solid-state asymmetric MHDs are one promising candidate with regard to safety and practical application. Therefore, we also assembled all-solid-state asymmetric MHDs with PVA-KOH gel electrolyte. As shown in Fig. 5a, d, the electrochemical performance of the all-solid-state asymmetric MHDs is clearly inferior that in 6 M KOH, which can be attributed to the limited ion penetration of the porous electrodes [29].

However, from the galvanostatic discharge curves (Fig. 5b), the areal capacitance of the all-solid-state asymmetric MHDs were calculated to be 28.5 mF cm^{-2} at a current density of 0.75 mA cm^{-2}. Furthermore, the all-solid-state asymmetric MHDs were placed in flat and different bending angles to evaluate their electrochemical performance by CV measurements at 50 mV s^{-1} (Fig. 5c). It can be observed that the device showed perfectly overlapped CV curves and negligible capacitance degradation at different bending angles, indicating the excellent mechanical stability and flexibility of the devices. To further demonstrate the advantage of the asymmetric MHDs, all-solid-state symmetric microsupercapacitors ($Ti_3C_2T_x$//$Ti_3C_2T_x$) with PVA-KOH gel electrolyte were also assembled for comparison. The CV curves (Fig. S7a) show a quasi-rectangular shape due to the intercalation pseudocapacitance of $Ti_3C_2T_x$. The areal capacitance of the symmetric microsupercapacitors calculated from the galvanostatic discharge curves shown in Fig. S7b reached 25.0 mF cm^{-2} at 0.75 mA cm^{-2}. Comparing the CV curves (Fig. 5d) of the asymmetric MHDs and symmetric microsupercapacitors, it can be observed that the asymmetric MHDs possess a wider operation potential window compared to the symmetric devices. High potential window range of the asymmetric MHDs makes it possible to provide high energy density, which is a very important parameter for the practical application of the energy storage devices. As the long-term stability is an important requirement for MHDs application, the cycling performance of all-solid-state asymmetric MHDs presented in Fig. 5e was evaluated at a current density of 1.25 mA cm^{-2}. 92 % of the initial capacitance remained after 10,000 cycles, demonstrating the remarkable reversibility and stability of the as-assembled all-solid-state asymmetric MHDs. Moreover, the electrochemical performance of asymmetric MHDs fabricated by screen-printing method was compared with other state-of-the-art MXene-based microsupercapacitors, as shown in the Ragone plot in Fig. 5f. The energy densities of both asymmetric (10.80 and 8.84 μWh cm^{-2} for asymmetric MHDs in 6M KOH and with PVA-KOH, respectively) and symmetric MXene-based

microsupercapacitors (1.25 μWh cm^{-2}) in this work are higher than that of the laser patterned MXene-based microsupercapacitors on paper (0.71 μWh cm^{-2}) [10], all-MXene microsupercapacitors on chip (0.67 μWh cm^{-2}) [11], and asymmetric flexible MXene//rGO microsupercapacitor [44] (see Table S1 and S2 for the data and standard deviation results in Supporting Information). The effective electrochemical performance demonstrates that fabricating asymmetric MHDs by modified two-step screen-printing method can be a simple, scalable, and efficient approach to improve the energy density.

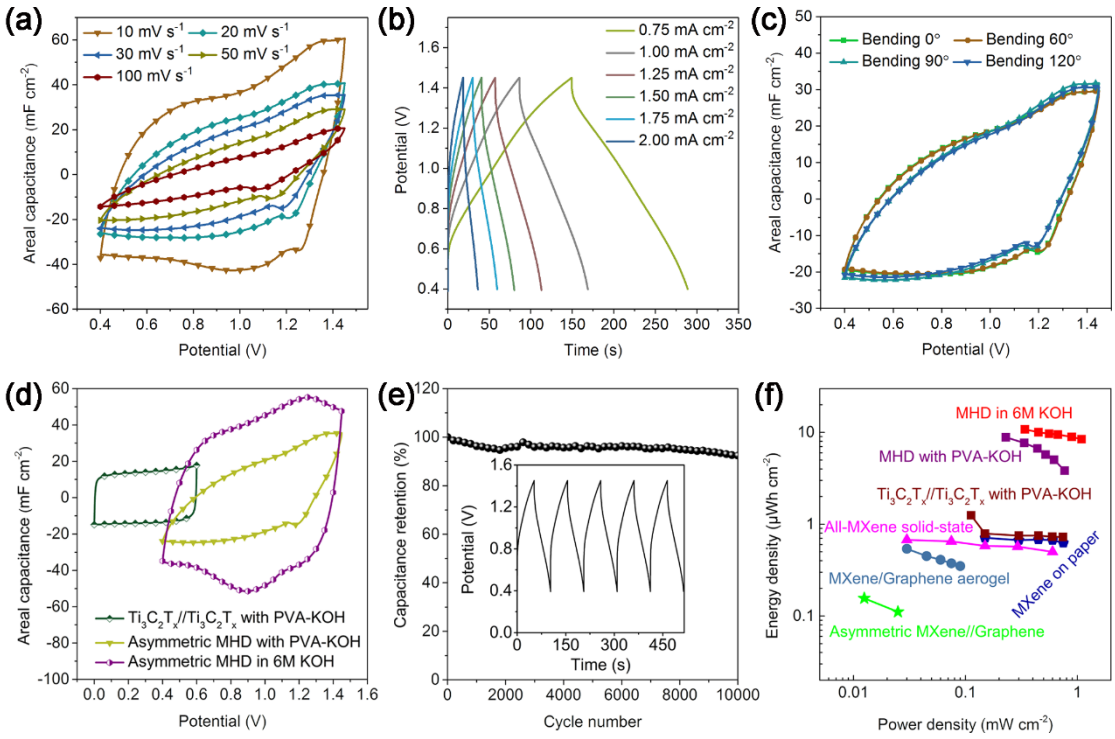

Fig. 5. (a) CV curves of the all-solid-state asymmetric MHDs with PVA-KOH gel electrolyte at different scan rates. (b) GCD curves of the all-solid-state asymmetric MHDs at different current densities. (c) CV curves of the all-solid-state asymmetric MHD at 30 mV s^{-1} collected at different bending angles. (d) Comparison of CV curves for the symmetric microsupercapacitors ($Ti_3C_2T_x$//$Ti_3C_2T_x$) with PVA-KOH gel electrolyte, asymmetric MHDs with PVA-KOH gel electrolyte and asymmetric MHDs in 6 M KOH electrolyte at a scan rate of 30 mV s^{-1}. (e) The cyclic performance of the all-solid-state coplanar asymmetric MHDs with PVA-KOH gel electrolyte. The inset is the last five charge-discharge cycles at 1.25 mA cm^{-2}. (f) Ragone plots of the

fabricated asymmetric coplanar devices and other state-of-the-art MXene-based coplanar microsupercapacitors from the literature.

Although many coplanar MHDs have been reported previously, their practical application in portable electronic devices is still a challenge and seldom demonstrated. Broad potential window and high energy density allow the screen-printed asymmetric MHDs to serve as suitable power source units for portable integrated electronic devices. With the aim of developing the practical application of the asymmetric MHDs, we integrated the force sensor (force sensing resistors) into the coplanar asymmetric MHD circuit to fabricate integrated devices. The force sensor is a polymer thick film device which exhibits a decrease in resistance with an increase in the force applied to the active surface. The force versus resistance characteristic shown in Fig. S8 provides an overview of the force sensor typical response behavior. As shown in Fig. 6a, the force sensor was connected in series with an all-solid-state asymmetric MHD. Electrochemical workstations were used to charge up the MHD and collect the response current to the force applied to the active surface. The digital photographs of the all-solid-state integrated devices on paper and PET substrates are shown in Fig. 6b. The self-discharge curves of the asymmetric MHDs with PVA-KOH gel electrolyte were presented in Fig. 6c. After 1000 s the open-circuit voltage can remain 1.0 V, which demonstrates the feasibility to use the asymmetric MHDs as power source to drive the force sensor. Different force with a frequency of 0.1 Hz was applied on the integrated sensor powered by the asymmetric MHD. The recorded current response was shown in Fig. 6d, from which it can be observed that the asymmetric MHD can serve as stable power source for the integrated sensor. Furthermore, Fig. 6e presented the current response for integrated sensor powered by a constant voltage of 1.0 V. As shown in Fig. 6f, the response current proportionally increases with the increasing of applied force on the active surface. Comparing the performance of the force sensor powered by an asymmetric MHD with that of a constant voltage, the obtained results further confirmed the feasibility of

employing the asymmetric MHDs as a substitute for a conventional energy unit to drive the force sensor. To further prove that the MHD can provide a stable output current to the force sensor, when used as an energy supply device, the output current curves of the MHD under different loads (33, 82 and 100 kOhm) taking into account the impedance match with the force sensor under different applied forces were measured (Fig. 6g), demonstrating that the output current remained relatively stable for 1000 s. In addition, it is worth mentioning that the integrated devices can be directly attached to human skin. The integrated sensor can also be used to detect the weak vibration of the arteries in fingers to measure heart rate. The measured live heartbeat waveform was shown in Fig. 6h, and the heart rate was calculated about 63 bpm. All of the above experimental results suggest the screen-printed asymmetric MHDs can be used as power source units for portable electronic devices and medical micro-devices.

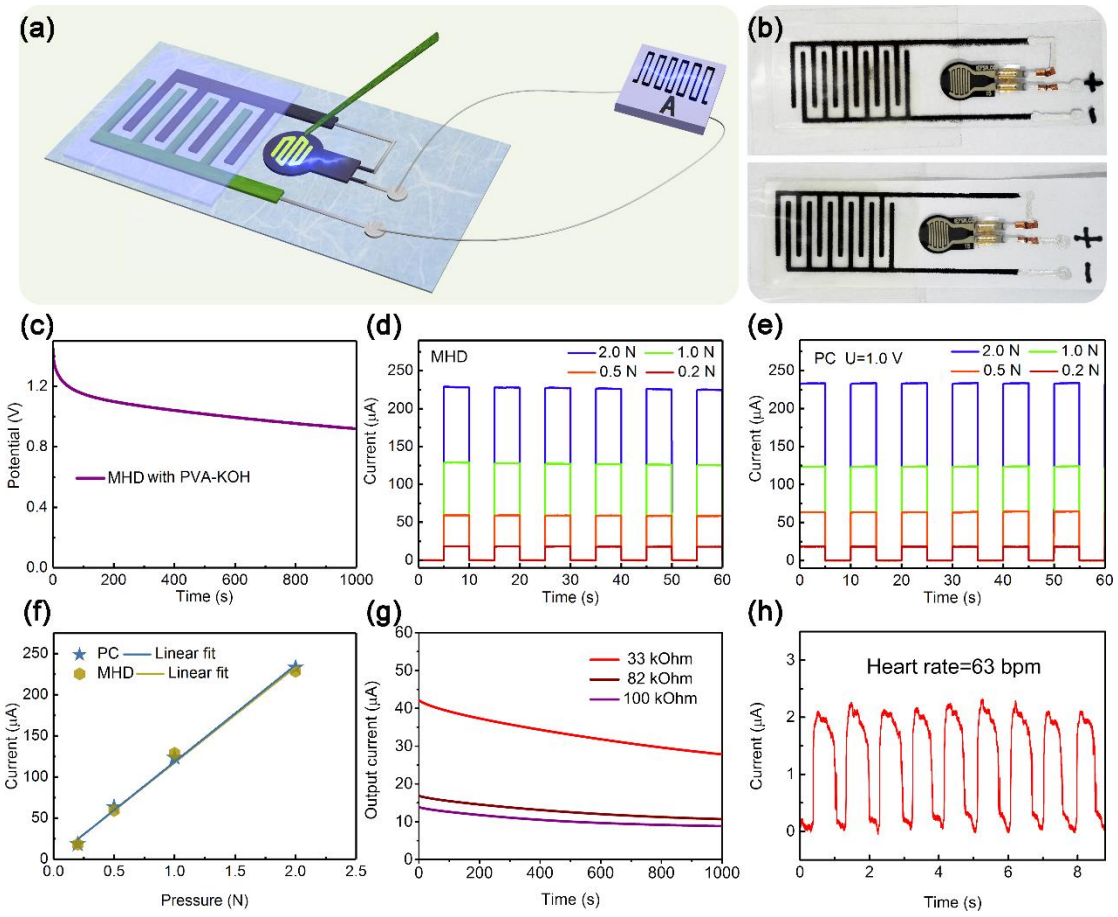

Fig. 6. (a) The schematic illustration of the electric circuit of the integrated force sensor. (b) The photographs of the integrated force sensors on paper and PET substrates. (c) The self-discharge curve of the asymmetric MHDs with PVA-KOH gel electrolyte. (d) The response current versus time plots of the integrated force sensor driven by an asymmetric MHD under different applied force on the active surface. (e) The response current versus time plots of the integrated force sensor at a bias of 1.0 V supplied by an external power source under different applied force. (f) The response current versus applied force plots of the integrated force sensor devices at a bias of 1.0 V and driven by an asymmetric MHD, respectively. The line shows linear fitting of the results. (g) The output current curves of the MHDs under different loads (33, 82 and 100 kOhm). (h) The measured live heartbeat waveform showing the heart rate of about 63 bpm.

4. Conclusions

In summary, coplanar asymmetric MHDs were fabricated by two-step screen-printing, which is a simple, cost-effective, and high throughput fabrication method, and can also be extended to other classes of materials for fabrication of coplanar asymmetric MHDs on various substrates. The screen-printed asymmetric MHDs present many advantages including outstanding cycling stability (92% retention of areal capacitance after 10,000 cycles), broadened potential window (1.45 V), enhanced energy density (10.80 and 8.84 μWh cm^{-2} for asymmetric MHDs in 6 M KOH and with PVA-KOH, respectively), light weight, and excellent mechanical flexibility. Moreover, as a stable power source unit, the fabricated asymmetric MHDs can also be integrated with force sensors to detect the applied pressure variation. The two-step screen-printing method opens up new avenues toward developing flexible coplanar asymmetric MHDs and this study promotes the application of MHDs based on MXenes for novel portable integrated electronic devices.

Acknowledgements

The authors sincerely acknowledge financial support from the General Programs of the National Natural Science Foundation of China (NSFC Grant No.21571080), the national long-term project (WQ20152200273) of "Thousand Talents Plan of Bureau of Foreign Experts Affairs" of People's Republic of China, and the Natural Science Foundation of Jilin province (20170101193JC).

References

[1] M. Beidaghi, Y. Gogotsi, Energy Environ. Sci. 7 (2014) 867-884.

[2] S. Gu, Z. Lou, L. Li, Z. Chen, X. Ma, G. Shen, Nano Res. 9 (2016) 424-434.

[3] L. Dong, C. Xu, Y. Li, Z. Pan, G. Liang, E. Zhou, F. Kang, Q. H. Yang, Adv. Mater. 42 (2016) 9313-9319.

[4] M. Létiche, E. Eustache, J. Freixas, A. Demortière, V. D. Andrade, L. Morgenroth, P. Tilmant, F. Vaurette, D. Troadec, P. Roussel, T. Brousse, C. Lethien, Adv. Energy Mater. 7 (2017) 1601402.

[5] A. R. Jiménez, R. Klöpsch, R. Wagner, U. C. Rodehorst, M. Kolek, R. Nölle, M. Winter, T. Placke, ACS Nano 11 (2017) 4731-4744.

[6] J. W. Long, B. Dunn, D. R. Rolison, H. S. White, Chem. Rev. 104 (2004) 4463-4492.

[7] W. Gao, N. Singh, L. Song, Z. Liu, A. L. M. Reddy, L. Ci, R. Vajtai, Q. Zhang, B. Wei, P. M. Ajayan, Nat. Nanotechnol. 6 (2011) 496-500.

[8] M. F. El-Kady, V. Strong, S. Dubin, R. B. Kaner, Science 335 (2012) 1326-1330.

[9] H. Li, Y. Hou, F. Wang, M. R. Lohe, X. Zhuang, L. Niu, X. Feng, Adv. Energy Mater. 7 (2016) 1601847.

[10] N. Kurra, B. Ahmed, Y. Gogotsi, H. N. Alshareef, Adv. Energy Mater. 6 (2016) 1601372.

[11] Y. Y. Peng, B. Akuzum, N. Kurra, M. Q. Zhao, M. Alhabeb, B. Anasori, E. C. Kumbur, H. N. Alshareef, M. D. Gerc, Y. Gogotsi, Energy Environ. Sci. 9 (2016) 2847-2854.

[12] X. Liu, T. Qian, N. Xu, J. Zhou, J. Guo, C. Yan, Carbon 92 (2015) 348-353.

[13] J. Lin, Z. Peng, Y. Liu, F. Ruiz-Zepeda, R. Ye, E. L. G. Samuel, M. J. Yacaman, B. I. Yakobson, J. M. Tour, Nat. Commun. 5 (2014) 5714.

[14] D. Pech, M. Brunet, P. L. Taberna, P. Simon, N. Fabre, F. Mesnilgrente, V. Conédéra, H. Durou, J. Power Sources 195 (2010) 1266-1269.

[15] P. Huang, C. Lethien, S. Pinaud, K. Brousse, R. Laloo, V. Turq, M. Respaud, A. Demortière, B. Daffos, P. L. Taberna, B. Chaudret, Y. Gogotsi, P. Simon, Science 351 (2016) 691-695.

[16] D. Pech, M. Brunet, H. Durou, P. Huang, V. Mochalin, Y. Gogotsi, P. L. Taberna, P. Simon, Nat. Nanotechnol. 5 (2010) 651-654.

[17] L. Zhang, D. DeArmond, N. T. Alvarez, R. Malik, N. Oslin, C. McConnell, P. K. Adusei, Y. Y. Hsieh. V. Shanov, Small 13 (2017) 1603114.

[18] A. Ponrouch, S. Garbarino, E. Bertin, D. Guay, J. Power Sources 221 (2013) 228-231.

[19] H. Wu, K. Jiang, S. Gu, H. Yang, Z. Lou, D. Chen, G. Shen, Nano Res. 8 (2015) 3544-3552.

[20] J. Yang, C. Yu, X. Fan, Z. Ling, J. Qiu, Y. Gogotsi, J. Mater. Chem. A 1 (2013) 1963-1968.

[21] B. Anasori, M. R. Lukatskaya, Y. Gogotsi, Nat. Rev. Mater. 2 (2017) 16098.

[22] L. Qin, Q. Tao, A. E. Ghazaly, J. Fernandez-Rodriguez, P. O. A. Persson, J. Rosen, F. Zhang, Adv. Funct. Mater. 28 (2018) 1703808.

[23] Q. Tao, M. Dahlqvist, J. Lu, S. Kota, R. Meshkian, J. Halim, J. Palisaitis, L. Hultman, M. W. Barsoum, P. O. A. Persson, J. Rosen, Nat. Commun. 8 (2017) 14949.

[24] P. Eklund, J. Rosen, P. O. A. Persson, J. Phys. D: Appl. Phys. 50 (2017) 113001.

[25] V. M. H. Ng, H. Huang, K. Zhou, P. S. Lee, W. Que, J. Z. Xu, L. B. Kong, J. Mater. Chem. A 5 (2017) 3039-3068.

[26] V. Augustyn, J. Come, M. A. Lowe, J. W. Kim, P. L. Taberna, S. H. Tolbert, H. D. Abruña, P. Simon, B. Dunn, Nat. Mater. 12 (2013) 518-522.

[27] M. Ghidiu, M. R. Lukatskaya, M. Q. Zhao, Y. Gogotsi, M. W. Barsoum, Nature 516 (2014) 78-81.

[28] M. R. Lukatskaya, B. Dunn, Y. Gogotsi, Nat. Commun. 7 (2016) 12647.

[29] Q. Jiang, N. Kurra, C. Xia, H. N. Alshareef, Adv. Energy Mater. 7 (2016) 1601257.

[30] M. F. El-Kady, M. Ihns, M. Li, J. Y. Hwang, M. F. Mousavi, L. Chaney, A. T. Lech, R. B. Kaner, Proc. Natl. Acad. Sci. 112 (2015) 4233-4238.

[31] Z. Lu, W. Zhu, X. Lei, G. R. Williams, D. O'Hare, Z. Chang, X. Sun, X. Duan, Nanoscale 4 (2012) 3640-3643.

[32] P. Vialat, C. Mousty, C. Taviot-Gueho, G. Renaudin, H. Martinez, J. C. Dupin, E. Elkaim, F. Leroux, Adv. Funct. Mater. 24 (2014) 4831-4842.

[33] Z. Gao, C. Bumgardner, N. Song, Y. Zhang, J. Li, X. Li, Nat. Commun. 7 (2016) 11586.

[34] M. Li, J. P. Cheng, J. Wang, F. Liu, X. B. Zhang, Electrochim. Acta 206 (2016) 108-115.

[35] Y. Xu, M. G. Schwab, A. J. Strudwick, I. Hennig, X. Feng, Z. Wu, K. Müllen, Adv. Energy Mater. 3 (2013) 1035-1040.

[36] K. Jost, D. Stenger, C. R. Perez, J. K. McDonough, K. Lian, Y. Gogotsi, G. Dion, Energy Environ. Sci. 6 (2013) 2698-2705.

[37] W. Liu, C. Lu, X. Wang, R. Y. Tay, B. K. Tay, ACS Nano 9 (2015) 1528-1542.

[38] O. Mashtalir, M. Naguib, V. N. Mochalin, Y. Dall'Agnese, M. Heon, M. W. Barsoum, Y. Gogotsi, Nat. Commun. 4 (2013) 1716.

[39] Z. Niu, Y. Li, Chem. Mater. 26 (2014) 72-83.

[40] J. Ji, L. L. Zhang, H. Ji, Y. Li, X. Zhao, X. Bai, X. Fan, F. Zhang, R. S. Ruoff, ACS Nano 7 (2013) 6237-6243.

[41] L. Li, S. Peng, H. B. Wu, L. Yu, S. Madhavi, X. W. Lou, Adv. Energy Mater. 5 (2015) 1500753.

[42] L. Xie, F. Su, L. Xie, X. Li, Z. Liu, Q. Kong, X. Guo, Y. Zhang, L. Wan, K. Li, C. Lv, C. Chen, ChemSusChem 8 (2015) 2917-2926.

[43] D. P. Dubal, O. Ayyad, V. Ruiz, P. Gomez-Romero, Chem. Soc. Rev. 44 (2015)

1777-1790.

[44] C. Couly, M. Alhabeb, K. L. V. Aken, N. Kurra, L. Gomes, A. M. Navarro-Suárez, B. Anasori, H. N. Alshareef, Y. Gogotsi, Adv. Electron. Mater. 4 (2017) 1700339.

Shuaikai Xu received his B.S. in Physics from Jilin University and Tomsk Polytechnic University in 2014. Shuaikai is currently a 2st year Ph.D. student at the Key Laboratory of Physics and Technology for Advanced Batteries (Ministry of Education), Jilin University, advised by Dr. Wei Han. His current research focuses on developing electrode materials based on two-dimensional metal carbides (MXenes) for supercapacitors.

Yohan Dall'Agnese is an Associate Professor at the Key Laboratory of Physics and Technology for Advanced Batteries at Jilin University. He received his Ph.D. in Materials Science and Engineering from Paul Sabatier University and Drexel University in 2016. Prior to joining Jilin University, he held a Postdoctoral appointment in the Faculty of Textile Science and Technology at Shinshu University. His research interests lie in the synthesis and characterization of two-dimensional nanomaterials for energy storage and conversion applications.

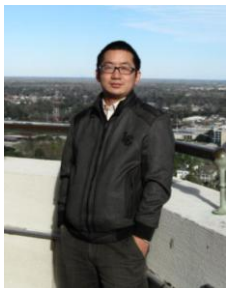

Guodong Wei is an associate professor in Jilin University. He received Ph.D. degree in Jilin University. At present, his major researches are low dimension nanomaterials-based optoelectronic nanodevices and energy storage devices.

Chao Zhang is a master candidate with the supervision of Prof. Wei Han at the Key Laboratory of Physics and Technology for Advanced Batteries (Ministry of Education), Jilin University. His current research focuses on developing composite electrode materials based on two-dimensional metal carbides (MXenes) for energy storage.

Yury Gogotsi is Distinguished University Professor of Materials Science and Engineering at Drexel University and Director of the A.J. Drexel Nanomaterials Institute. His Ph.D. is in physical chemistry from Kiev Polytechnic and D.Sc. in Materials Engineering from Ukrainian Academy of Sciences. He works on MXenes

and nanostructured carbons for energy related and other applications. He has more than 500 journal papers and obtained more than 50 patents. He has received numerous national and international awards for his research and was elected a Fellow of AAAS, MRS, RSC, ECS and ACerS, and a member of the World Academy of Ceramics.

Wei Han is a Professor at College of Physics, Jilin University. He is also the Executive Deputy Director of the International Center of Future Science, Jilin University. He received his Ph.D. in Solid-State Physics from Tomsk Polytechnic University in 1997. He works on the application of supercapacitor in the fields of electric vehicles and new energy resource (solar and wind energy), design of electrode materials for producing hydrogen by electrolysed water, and application of nanomaterials in the field of nuclear wastewater purification. He has more than 50 journal papers, and obtained more than 20 patents.